Multiphoton microscopy observations of 3D elastin and collagen fiber microstructure changes during pressurization in aortic media

Shukei Sugita and Takeo Matsumoto*, *Nagoya, Japan*

Affiliation:

Biomechanics Laboratory, Department of Mechanical Engineering, Graduate School of Engineering, Nagoya Institute of Technology

*Current: Department of Mechanical Science and Engineering, Graduate School of Engineering, Nagoya University

To whom correspondence should be addressed:

Shukei Sugita, Ph.D.

Department of Mechanical Engineering, Graduate School of Engineering, Nagoya Institute of Technology

Gokiso-cho, Showa-ku, Nagoya 466-8555, JAPAN

Tel. and Fax: +81 52 735 7125

E-mail: sugita.shukei@nitech.ac.jp

Key Words: Thoracic Aorta, Waviness, Second Harmonic Generation, Two-photon Microscopy

Abstract (150–250 words)

Elastin and collagen fibers play important roles in the mechanical properties of aortic media. Because knowledge of local fiber structures is required for detailed analysis of blood vessel wall mechanics, we investigated 3D microstructures of elastin and collagen fibers in thoracic aortas and monitored changes during pressurization. Using multiphoton microscopy, autofluorescence images from elastin and second harmonic generation signals from collagen were acquired in media from rabbit thoracic aortas that were stretched biaxially to restore physiological dimensions. Both elastin and collagen fibers were observed in all longitudinal–circumferential plane images, whereas alternate bright and dark layers were observed along the radial direction and were recognized as elastic laminas (ELs) and smooth muscle-rich layers (SMLs), respectively. Elastin and collagen fibers are mainly oriented in the circumferential direction, and waviness of collagen fibers was significantly higher than that of elastin fibers. Collagen fibers were more undulated in longitudinal than in radial direction, whereas undulation of elastin fibers was equibiaxial. Changes in waviness of collagen fibers during pressurization were then evaluated using 2 dimensional fast Fourier transform in mouse aortas, and indices of waviness of collagen fibers decreased with increases in intraluminal pressure. These indices also showed that collagen fibers in SMLs became straight at lower intraluminal pressures than those in EL, indicating that SMLs stretched more than ELs. These results indicate that deformation of the aorta due to pressurization is complicated because of the heterogeneity of tissue layers and differences in elastic properties of ELs, SMLs, and surrounding collagen and elastin.

INTRODUCTION

Aortic media predominantly comprises smooth muscle cells (SMCs) and extracellular matrix (ECM) proteins such as elastin and collagen fibers. Elastic laminas (ELs) containing elastin alternate with smooth muscle-rich layers (SMLs) in the radial direction and collagen fibers are present around SMCs and in ELs (Clark and Glagov 1985). Young's moduli of elastin (approximately 0.6 MPa) and collagen fibers (approximately 1 GPa; (Fung 1993) are comparable with those of aortas in low and high pressure regions, respectively (Wagenseil and Mecham 2009). In agreement, elastin and collagen fibers have been considered principal load-bearing elements in low and high pressure regions, respectively. Low contributions of collagen to mechanical properties in low pressure regions can be explained by waviness of collagen fibers under low pressure, and gradual straightening under pressure (Roy et al. 2010). However, neither three-dimensional structures of elastin and collagen fibers, nor their deformations during pressurization, have been described in detail. Hence, to investigate blood vessel wall mechanics, knowledge of local fiber structures is required. Microstructures of elastin and collagen in media have mostly been investigated using histology and electron microscopy. However, these methods are not suitable for observations of three-dimensional microstructures of elastin and collagen, or their deformations during physiological loading.

Multiphoton microscopy (MPM) has been used for simultaneous observations of collagen and elastin fibers in aortas (Boulesteix et al. 2006; Chow et al. 2014; Phillippi et al. 2014; Tsamis et al. 2013; Zeinali-Davarani et al. 2015). Moreover, autofluorescence from elastin and second harmonic generation (SHG) signals from collagen can be observed in MPM images. Hence, fiber directions (Phillippi et al. 2014; Tsamis et al. 2013), changes in fiber direction under biaxial stretch conditions (Chow et al. 2014; Zeinali-Davarani et al. 2015), and relation between delamination strength and microstructure of collagen in the radial direction (Pal et al. 2014) have been investigated using this technique. In addition, because this method does not require staining or fixation of tissues, deformation of specimens and changes in fiber structure can be observed during stretching. Although collagen and elastin have been observed using MPM in multiple studies, microscopic 3D structures of these fibers have not been well investigated. In addition, collagen fiber structures in media remain poorly understood, perhaps

reflecting weak SHG collagen fiber signals. However, elastin and collagen fibers play vital roles in the mechanical properties of aortic media, because the elastic modulus of the media is higher than that of elastin under conditions of large deformation.

In this study, we investigated the three-dimensional microstructures of elastin and collagen fibers in aortic media using MPM. After optimizing image acquisition systems to obtain clear images of collagen fibers in the media, 3D microstructures and spatial arrangements of elastin and collagen fibers were observed in the aorta. Changes in waviness of collagen fibers during pressurization were then investigated quantitatively and microscopic deformations of aortas following pressurization are discussed.

MATERIALS AND METHODS

Sample preparation

All animal experiments were approved by the institutional review board for animal care at Nagoya Institute of Technology, and were performed in accordance with the *Guide for Animal Experimentation, Nagoya Institute of Technology*.

To observe 3D microstructures of elastin and collagen fibers, rabbit thoracic aortas were obtained according to previously described methods (Matsumoto et al. 1995). Briefly, three male Japanese white rabbits weighing 3.3–3.5 kg were sacrificed using overdoses of sodium pentobarbital. After marking vessels with dots of saturated gentian violet solution at 5-mm intervals, *in vivo* lengths were estimated, and tubular segments of 25 mm were resected from the descending thoracic aorta and were cut into rectangular specimens. Specimens were stretched to *in vivo* lengths in the longitudinal direction and by 60% in the circumferential direction, corresponding to a blood pressure of 80 mmHg (Sugita et al. 2003), and were pinned on a cork-board at their edges. Relative spatial arrangements of elastin and collagen fibers were then observed in rabbit specimens.

Although collagen and elastin fibers can be observed in detail using MPM, the resulting images lack sufficient clarity in regions deeper than approximately 60 μm from the surface, which corresponds to two ELs plus one or two SMLs. Thus, 200-μm thick rabbit thoracic aortas were inappropriate for observations of whole wall thicknesses, and mouse

thoracic aortas were used instead, although the quality of MPM image was not as good as rabbit aorta. Four male Slc:ddY mice weighing approximately 35 g were sacrificed by exposure to carbon dioxide. After marking the descending thoracic aorta with dots at 5 mm intervals as stated above, intercostal arteries were cauterized, and tubular segments of 15 mm were resected and immersed in PBS(−) solution at 4°C until experiments. Changes in waviness of collagen fibers during pressurization were then monitored in mouse aortas.

Multiphoton and SHG microscopy

Experiments were performed with a multiphoton laser scanning microscope (FV1200MPE, Olympus, Tokyo, Japan) equipped with a mode locked Ti:sapphire laser (pulse width = 100 fs, repetition frequency = 80 MHz, and wavelength = 800 nm; MaiThai, Spectra Physics, Santa Clara, CA, USA). Optical devices (Dichroic mirror, 485 nm; band-pass filter for fluorescence, 495–540 nm; band-pass filter for SHG, 400 ± 5 nm) were used with an objective lens (LUMPLFLN 60XW, NA = 1.00 or UPLSAPO 60XW, NA = 1.20, Olympus), and preliminary experiments confirmed the ability of this system to produce clear images of elastin and collagen fibers (see supplemental material S1). Laser was introduced as circular polarized light and SHG signal was collected in the backwards direction to minimize the effects of fiber orientation and organization on the image.

Because collagen fibers were aligned in the longitudinal–circumferential plane in media from thoracic aortas (Schriefl et al. 2011), images of aortic tissues were captured in the plane perpendicular to the radial direction. Images in the circumferential–longitudinal plane of rabbit aortic specimens were acquired at 1 μm intervals from the intima to a depth of approximately 60 μm in the radial direction from the intimal side. Laser power was increased from 1% at the surface of the specimen to 10% at deep planes so that clear images could be acquired at deep planes.

To distinguish the EL and SML in SHG and autofluorescent images from their intensities, cell nuclei were stained because cell nuclei are only in SMLs. A specimen of the rabbit thoracic aorta was immersed in 5 μg/mL Hoechst 33342 (Life Technologies, Carlsbad, CA, USA) for 1 h to identify positions of SMC nuclei, and were observed using MPM with a

filter cube (Dichroic mirror, 485 nm; band-pass filters, 420–460 nm and 495–540 nm) and a laser wavelength of 900 nm.

Pressurization of the aortas using the MPM

Tubular segments of mouse thoracic aortas were pressurized under a microscope using the experimental apparatus shown in Fig. 1. Both ends of the tubular segments were tied around 22G hypodermic needles using suture threads and segments were placed in a tissue bath containing PBS(−) at room temperature. One needle was occluded and another was connected to a syringe and a manometer through a reservoir. After stretching to its *in vivo* length with reference to the dots, specimens were pressurized at a rate of 5 mL/min with a syringe pump (CX07200, ISIS, Osaka, Japan) under a multiphoton microscope. Pressurization was stopped at every 20 mmHg, and images of specimens were acquired as stated in the previous section.

Image analyses

All image analyses were performed using ImageJ 1.47v software (National Institutes of Health, Bethesda, MD, USA).

Elastin and collagen fibers tended to align in the circumferential direction rather than in the longitudinal direction (Chow et al. 2014). Thus, for 3D structure analyses of elastin and collagen fibers, images were stacked perpendicular to the radial direction (211 × 211 μm^2 at 1 μm intervals) of rabbit aortic tissues (Fig. 2a), and were obtained and cropped so that fiber lengths were approximately 20 μm (Fig. 2b) to select fibers without bifurcation or connecting points with other fibers. Images on the plane perpendicular to the circumferential direction were then obtained by reslicing at 0.41-μm intervals (Fig. 2c). Centers of each fiber were identified as the point of local maximum intensity on each image using the “Find Maxima” function (Fig. 2d and 2e). Fiber lengths were then calculated in image stacks that were perpendicular to the circumferential direction by adding all distances between adjacent center points (Fig. 2f). Distances between center points at i^{th} and $i + 1^{th}$ slices were calculated as follows:

$$d_i = \sqrt{(Long_i - Long_{i+1})^2 + (Rad_i - Rad_{i+1})^2 + (Circ_i - Circ_{i+1})^2}\ , \quad (1)$$

where, *Long*, *Rad*, and *Circ* are the coordinates in longitudinal, radial, and circumferential directions, respectively. Accordingly, fiber length *L* was calculated by adding all distances from 1st to *n*th slices as follows:

$$L = \sum_{i}^{n-1} d_i \quad (2)$$

Waviness *w* was calculated by dividing the fiber length *L* by the distance between center points in the first and the last slices using the following equation:

$$w = \frac{L}{\sqrt{(Long_1 - Long_n)^2 + (Rad_1 - Rad_n)^2 + (Circ_1 - Circ_n)^2}} \quad (3)$$

Standard deviations of center-point displacements in longitudinal and radial directions were measured to estimate directions of fiber undulations. Projection images in the circumferential direction were also obtained for each fiber. Fiber images were captured at five locations per animal, and nine segments of fibers were selected in these locations at various slices and depth. Thus, 27 segments in total were analyzed from three rabbits.

Changes in waviness of collagen fibers during pressurization were analyzed using 2 dimensional fast Fourier transform (2D-FFT) (Petroll et al. 1993) in images of mouse aortas as follows: At each pressure, five 30 × 30 μm^2 areas were selected perpendicular to the radial direction (Fig. 3a) and images of these areas were processed using 2D-FFT to obtain power spectrum images (PSI). PSI represents the amplitude of the power spectrum of the input image at space frequency *R* in the direction φ as gray values in polar coordinates (R, φ; Fig. 3b). Because high intensities were observed in directions that were perpendicular to the directions of fibers (Petroll et al. 1993), the orientation angle of the collagen fibers α was represented as follows:

$$\alpha = \varphi + 90^\circ \quad (4)$$

We calculated mean gray values of the areas from 0° to 180° every 10° around the origin, normalized them by their sum, and determined distributions of fiber orientations (Fig. 3c). Angles > 180° were expressed in the range $0° \le \alpha < 180°$ by subtracting 180°. To quantify fiber orientations, probability distributions of fiber orientations were fitted using the following

Gaussian function:

$$P = P_{base} + (P_{peak} - P_{base}) \exp\left\{\frac{-(\alpha - \alpha_{average})^2}{2\sigma^2}\right\}, \quad (5)$$

where P is the probability of fiber angle α, and P_{base}, P_{peak}, $\alpha_{average}$, and σ are fitting constants that indicate base levels, maximum values, average angles, and standard deviations (SD) of Gaussian distributions, respectively (Fig. 3c). We found that lower waviness causes higher P_{peak} values in the probability distributions obtained in 2D-FFT (See supplemental material S2 for details). Hence, these fitting constants, especially parameters P_{peak} and σ, were used as indices of fiber waviness.

Statistics

Data are presented as mean ± SD. Changes in the P_{base}, P_{peak}, $\alpha_{average}$, and σ with pressure were evaluated using Pearson's correlation constants. Differences between two groups were identified using Student's paired and unpaired t-test for one and independent two samples, respectively. Differences were considered statistically significant when $P < 0.05$ in all tests.

RESULTS AND DISCUSSION

Appearance of elastin and collagen fibers obtained with the MPM

Figure 4 (a–i) shows elastin, collagen, and their merged images in the longitudinal–circumferential plane in a rabbit thoracic aorta at various radial positions (See also Movie S1). The radial position was moved from intimal to adventitial sides, leading to alternate appearances of bright and dark regions, whereas the radial–longitudinal plane image clearly shows the layered structure of elastin and collagen fibers in the radial direction (Fig. 4j). Comparisons of these images with histological sections stained with Elastica van Gieson (data not shown) and with images of elastin and cell nuclei in longitudinal-radial (Fig. 4k) and longitudinal-circumferential plane (Fig. 3S) confirmed that bright (Z = 5, 33 μm) and dark (Z = 22 μm) regions corresponded with ELs and SMLs, respectively. In longitudinal-circumferential plane, elastin fibers tended to align in the circumferential direction in SMLs (Fig. 4b) whereas they often aligned in the longitudinal direction and connect to each other to

form network structure in ELs (Fig. 4c).

Elastin and collagen fibers that were oriented in the longitudinal direction were prominent in the sub-luminal space (Fig. 4a, 4d, and 4g), as reported in a previous study (Sato et al. 1994), but were oriented in the circumferential direction in deeper regions (Fig. 4b, 4e, 4h, 4c, 4f, and 4i), as is known widely. High-intensity layers in the elastin images from near the intraluminal surface (Fig. 4a) were considered internal elastic lamina (IEL). Although ELs have been observed as lamina in histological sections, these have fiber-like structures. Moreover, as indicated in panels (e) and (f), collagen fibers were observed more in ELs than in SMLs, indicating that ELs comprise elastin and collagen fibers. Elastin and collagen fibers were also found passing through fenestrations in IELs (Fig. 4a, 4d, and 4g, insets). In agreement, fenestrations and associated fiber-like structures have been observed in scanning electron microscope and confocal microscopy analyses (Arribas et al. 2008; Boumaza et al. 2001; Campbell and Roach 1981), whereas components of the fiber-like structure remained unclear. Hence, the present MPM analyses are the first to confirm that these fibers include both elastin and collagen.

3D microstructure of elastin and collagen fibers in aortic media

Figure 5a–5c shows a typical image of elastin and collagen fibers in SMLs of the media from rabbit thoracic aortas extended at physiological stretch ratios (longitudinal direction, approximately 1.3; circumferential direction, 1.6). Elastin fibers were less undulated than collagen fibers. Thus, to determine relative positions of elastin and collagen fibers and investigate waviness in further detail, we resliced 3D data in the longitudinal–radial plane and stacked resliced images to obtain fiber images that were projected to the plane perpendicular to the circumferential direction (Fig. 5d). These analyses confirmed that although undulated collagen fibers were close to elastin fibers, none of them were wound around elastin fibers (n = 27). We found similar trend in all animals, although the difference was not significant at $P < 0.05$ in some animals. Moreover, reconstructed images of 3D structures of fibers supported this finding (Movie S2), and deviations of displacement of the center positions of collagen fibers in the longitudinal direction were significantly greater than those in the radial direction

(Fig. 5e), indicating that collagen fibers undulated more in the longitudinal-circumferential plane than the radial-circumferential plane. These observations suggest that SMCs that reside between ELs may inhibit deformation of collagen fibers in the radial direction and limit undulation of collagen fibers in the longitudinal-circumferential plane. In contrast, no significant differences in directions of undulation were found for elastin fibers, and as shown in Fig. 5a, waviness of collagen fibers was significantly higher than that in elastin fibers (Fig. 5f).

Changes in collagen fiber undulation in aortic media during pressurization

Figure 6 shows typical SHG images of collagen fibers during pressurization in mouse thoracic aorta. Collagen fibers in mouse aortas were not as clearly observed as those in rabbit aortas, although the reason for this remains unknown. Moreover, dark and bright regions were observed (Fig. 4) and were considered SMLs and the ELs, respectively. Pressurized mouse aortas have cylindrical shapes with radii of approximately 1 mm and several SMLs and ELs were observed in a single slice, reflecting significant curvature of SMLs and ELs in optical slices. Accordingly, in the dark regions of SMLs, sparse collagen fibers were clearly observed at higher pressures, and appeared to undulate less at higher pressure than at lower pressure, and less in SMLs than in ELs.

These observations were confirmed in analyses of 2D-FFT images, and probability distributions of fiber orientations were generated (Fig. 7). Differences in distributions of fiber orientation were then evaluated using the parameters P_{base}, P_{peak}, $\alpha_{average}$, and σ in Eq. (5). Initially, distributions of fiber orientations (Fig. 7a) showed that most collagen fibers were aligned to 90° in all cases, indicating that the orientation of collagen fibers is predominantly circumferential, as corroborated by relative insensitivities of angles at maximum alignment $\alpha_{average}$ to pressure and region (Fig. 7b). Similarly, the base level of the fitted Gaussian function P_{base} decreased significantly with pressure increases in both bright and dark regions ($r = -0.96$ for the bright region, $r = -0.97$ for the dark region; Fig. 7c). Moreover, maximum values of the fitted Gaussian function P_{peak} increased significantly with the pressure increase in both regions ($r = 0.87$ for the bright region, $r = 0.94$ for the dark region, Fig. 7d). These data indicate that

collagen fibers become less undulated at higher pressures. In agreement, the maximum value P_{peak} was significantly higher in the dark region than in the bright region at 60–120 mmHg (Fig. 7d), and SDs of the Gaussian function σ were significantly lower in the dark region than in the bright region at 60–160 mmHg (Fig. 7e). These results indicate that collagen fibers became less wavy in SMLs than in ELs following pressure increases. In contrast, differences between ELs and SMLs were not significant for $\alpha_{average}$ and P_{base} except at 140 mmHg (Fig. 7b and 7c). Similar result was obtained in the rabbit aorta (Fig. S4). For elastin fibers, all four parameters, $\alpha_{average}$, P_{base}, P_{peak}, and σ changed similarly to collagen fibers with increase in pressure though their correlation coefficients of P_{base} and P_{peak} were significant only in dark region (Fig. S5). These results also support larger deformation in the SMLs than in the ELs.

The present data warrant speculation that collagen fibers in SMLs become less wavy at low pressure regions than in ELs, because initial fiber waviness is smaller in SMLs than in ELs at 0 mmHg. However, P_{peak} and σ did not differ significantly between ELs and SMLs at 20 and 40 mmHg (Fig. 7b and 7c), thus providing evidence against this hypothesis.

The observed differences in mechanical behaviors of collagen fibers in ELs and SMLs may be caused by differing elastic moduli of these tissues around collagen fibers (Fig. 8a). Accordingly, elastin is the main substance around collagen fibers in ELs, whereas SMCs predominate around SMLs. Moreover, the elastic moduli of elastin and SMCs are approximately 0.6 MPa (Fung 1993) and 0.01–0.1 MPa (Nagayama and Matsumoto 2004), respectively. Hence, when collagen fibers in SMLs are stretched due to pressurization, compliant SMCs around the collagen fibers may offer comparatively limited resistance to movements of collagen fibers, allowing collagen fibers to straighten without considerable stretching along their length ($L_{0\text{-}SML}$ under low pressure is almost the same as L_{SML} under high pressure in Fig 8a). In contrast, stiff elastin in ELs may resist movement of collagen fibers, ensuring that collagen fibers increase in length (fiber stretched from $L_{0\text{-}EL}$ under low pressure to L_{EL} under high pressure in Fig 8a) without marked straightening. Specifically, undulating fibers should become straight faster in response to macroscopic stretch when their length along the undulation does not change, potentially reflecting fast decrease in relative waviness of

collagen fibers during pressurization in SMLs.

An alternative mechanism for differences between mechanical behaviors of collagen fibers in SMLs and ELs may involve shear deformation of the wall in the circumferential direction (Fig. 8b). Because ELs are stiffer than SMLs (Matsumoto et al. 2004), shear strain is larger in SMLs than in ELs following deformation during pressurization. Accordingly, if arteries were thick-walled cylinders of homogeneous material, such deformations would not occur, whereas, shear deformation during pressurization has been observed frequently in rabbit thoracic aortas, as shown in Fig. S6. Although the ensuing driving forces remain unclear, such shear deformation may stretch collagen fibers in SMLs that bridge adjacent ELs (Fig. 8b, inset image).

Decrease in type I and increase in type III collagen correlated significantly with decrease in elastic modulus of tendon (Wan et al. 2014). This might indicate that collagen type I is stiffer than type III. McCullagh et al (1980) reported that collagen type I and III concentrated around SMCs and elastic laminas, respectively. Taken together, collagen may contribute more to the stiffening of the SMLs than that of the ELs. In reality, however, it has been reported that the ELs were much stiffer than the SMLs (Matsumoto et al. 2004). The reason for this discrepancy may be caused by the difference in collagen amount in the two layers. As shown in Fig. 4, the SMLs contain less amount of collagen fibers than the ELs do. This may cause the decrease in the elastic modulus in the SML, resulting in large strain and large change of waviness of collagen fibers between them.

Several papers have been published about change in collagen undulation during pressurization. Roy et al. (2010) observed the changes in waviness of collagen in media of rabbit left carotid artery stained with picrosirius red. In their study, samples were fixed at various pressures, and data from several animals were statistically analyzed. Schrauwen et al (2012) observed changes in waviness of collagen fibers in adventitia of rabbit common carotid artery under fluorescent microscope. Chow et al (2014) observed changes in waviness of collagen in media of porcine thoracic aorta during pressurization. The present study confirmed changes in collagen waviness in the whole media of mouse thoracic aorta.

Although collagen fibers in rabbit thoracic aortas could be clearly observed in this

study, fibers in mouse aortas could not (Fig. 9). Moreover, the image quality of collagen fibers in the mouse aortas was insufficient to analyze waviness directly, as performed in rabbit aortas, and 2D-FFT analyses were performed for mouse aortas. Although it is unclear why mouse image qualities were poor, images of rabbit aortas were obtained from the intimal side, whereas those of mouse aortas were obtained from the adventitial side to accommodate pressurized tests. Thus, much higher intensity in SHG images from adventitial tissues may have affected image clearness. However, elastin was not clearly observed in aortic media even though the elastin signal intensity in adventitia was much lower in mouse aortas. Finally, the images in Fig. 9 show differences in fiber structure between mice and rabbit aortas, and show wider fibers in the larger animal. Thus, differences in collagen fiber densities may be the cause of differences in clearness between animal models. In the present study, we did not find any difference between mice and rabbits. However, we should use caution in extrapolating results from rabbit aortas to mouse aortas, because there are anatomical differences in the aorta between them such as thicker wall, larger radius, more SMLs in rabbits.

In summary, we observed 3D microstructures of elastin and collagen fibers using MPM, and found that collagen fibers aligned in the circumferential direction were undulated more in longitudinal than in radial directions. Furthermore, waviness of collagen fibers was greater in ELs than in SMLs at physiological pressure levels, whereas the difference was insignificant at lower pressures, potentially reflecting differences in stiffness. These results indicate that deformation of the aorta due to pressurization is complicated by heterogeneity of tissue layers. Specifically, differences in elastic properties of ELs and SMLs and their surrounding collagen and elastin based interstitial may contribute to complex aortic tissue dynamics under pressure, warranting further investigations of the associated mechanisms and physiological relevance.

Conflict of interest statement

There are no conflicts of interest.

Acknowledgements

This work was supported in part by JSPS KAKENHIs (Nos. 22127008, 22240055, 26709002, and 15H02209) and special operational grants in Nagoya Institute of Technology.

References

Arribas SM et al. (2008) Heightened aberrant deposition of hard-wearing elastin in conduit arteries of prehypertensive SHR is associated with increased stiffness and inward remodeling Am J Physiol Heart Circ Physiol 295:H2299-H2307 doi:10.1152/ajpheart.00155.2008

Boulesteix T, Pena AM, Pages N, Godeau G, Sauviat MP, Beaurepaire E, Schanne-Klein MC (2006) Micrometer scale ex vivo multiphoton imaging of unstained arterial wall structure Cytometry A 69:20-26 doi:10.1002/cyto.a.20196

Boumaza S, Arribas SM, Osborne-Pellegrin M, McGrath JC, Laurent S, Lacolley P, Challande P (2001) Fenestrations of the Carotid Internal Elastic Lamina and Structural Adaptation in Stroke-Prone Spontaneously Hypertensive Rats Hypertension 37:1101-1107 doi:10.1161/01.hyp.37.4.1101

Campbell GJ, Roach MR (1981) Fenestrations in the internal elastic lamina at bifurcations of human cerebral arteries Stroke 12:489-496 doi:10.1161/01.str.12.4.489

Chow M-J, Turcotte R, Lin Charles P, Zhang Y (2014) Arterial Extracellular Matrix: A Mechanobiological Study of the Contributions and Interactions of Elastin and Collagen Biophysical Journal 106:2684-2692 doi:10.1016/j.bpj.2014.05.014

Clark JM, Glagov S (1985) Transmural organization of the arterial media. The lamellar unit revisited Arteriosclerosis 5:19-34 doi: 10.1161/01.ATV.5.1.19

Fung YC (1993) Biomechanics: Mechanical Properties of Living Tissues, second edition. In. Springer-Verlag, New York, pp 242-251

Matsumoto T, Goto T, Sato M (2004) Microscopic Residual Stress Caused by the Mechanical Heterogeneity in the Lamellar Unit of the Porcine Thoracic Aortic Wall JSME International Journal Series A Solid Mechanics and Material Engineering 47:341-348 doi:10.1299/jsmea.47.341

Matsumoto T, Hayashi K, Ide K (1995) Residual strain and local strain distributions in the rabbit atherosclerotic aorta J Biomech 28:1207-1217 doi:0021929094001798 [pii]

McCullagh KG, Duance VC, Bishop KA (1980) The distribution of collagen types I, III and V (AB) in normal and atherosclerotic human aorta J Pathol 130:45-55

doi:10.1002/path.1711300107

Nagayama K, Matsumoto T (2004) Mechanical Anisotropy of Rat Aortic Smooth Muscle Cells Decreases with Their Contraction (Possible Effect of Actin Filament Orientation) JSME international journal Series C, Mechanical systems, machine elements and manufacturing 47:985-991 doi:10.1299/jsmec.47.985

Pal S, Tsamis A, Pasta S, D'Amore A, Gleason TG, Vorp DA, Maiti S (2014) A mechanistic model on the role of "radially-running" collagen fibers on dissection properties of human ascending thoracic aorta J Biomech 47:981-988 doi: 10.1016/j.jbiomech.2014.01.005

Petroll WM, Cavanagh HD, Barry P, Andrews P, Jester JV (1993) Quantitative analysis of stress fiber orientation during corneal wound contraction J Cell Sci 104:353-363

Phillippi JA et al. (2014) Mechanism of aortic medial matrix remodeling is distinct in patients with bicuspid aortic valve J Thorac Cardiovasc Surg 147:1056-1064 doi:S0022-5223(13)00493-5 [pii]10.1016/j.jtcvs.2013.04.028

Roy S, Boss C, Rezakhaniha R, Stergiopulos N (2010) Experimental characterization of the distribution of collagen fiber recruitment J Biorheol 24:84-93 doi:10.1007/s12573-011-0027-2

Sato F, Shimada T, Kitamura H, Campbell GR, Ogata J (1994) Changes in morphology of elastin fibers during development of the tunica intima of monkey aorta Heart Vessels 9:140-147 doi:10.1007/BF01745239

Schrauwen JTC, Vilanova A, Rezakhaniha R, Stergiopulos N, van de Vosse FN, Bovendeerd PHM (2012) A method for the quantification of the pressure dependent 3D collagen configuration in the arterial adventitia Journal of Structural Biology 180:335-342 doi:10.1016/j.jsb.2012.06.007

Schriefl AJ, Zeindlinger G, Pierce DM, Regitnig P, Holzapfel GA (2011) Determination of the layer-specific distributed collagen fibre orientations in human thoracic and abdominal aortas and common iliac arteries J R Soc Interface 9:1275-1286 doi:10.1098/rsif.2011.0727

Sugita S, Matsumoto T, Sato M (2003) Local strain measurement of arterial wall based on

longitudinal observation Transactions of the Japan Society of Mechanical Engineers Series A 69:43-48 doi:10.1299/kikaia.69.43

Tsamis A et al. (2013) Fiber micro-architecture in the longitudinal-radial and circumferential-radial planes of ascending thoracic aortic aneurysm media J Biomech 46:2787-2794 doi:S0021-9290(13)00412-0 [pii]10.1016/j.jbiomech.2013.09.003

Wagenseil JE, Mecham RP (2009) Vascular extracellular matrix and arterial mechanics Physiol Rev 89:957-989 doi:10.1152/physrev.00041.2008

Wan C, Hao Z, Wen S, Leng H (2014) A Quantitative Study of the Relationship between the Distribution of Different Types of Collagen and the Mechanical Behavior of Rabbit Medial Collateral Ligaments PLoS ONE 9:e103363 doi:10.1371/journal.pone.0103363

Zeinali-Davarani S, Wang Y, Chow M-J, Turcotte R, Zhang Y (2015) Contribution of Collagen Fiber Undulation to Regional Biomechanical Properties Along Porcine Thoracic Aorta Journal of Biomechanical Engineering 137:051001 doi:10.1115/1.4029637

Figure legends

Fig. 1 Schematic of experimental apparatus for pressurization of aortas

Fig. 2 Schematic of methods for 3D analyses of elastin and collagen fibers

Images captured in the plane that is perpendicular to the radial direction (a); an area was cropped to include at least one elastin and one collagen fiber (b). The image was resliced to generate a plane that was perpendicular to the circumference (c) and centers of fibers were identified (d). Panel (e) shows merged images from panels (c) and (d). Fiber lengths were determined as the sum of distances between center points of all neighboring slices (f).

Fig. 3 Procedure for quantifying changes in fiber waviness

(a) A typical second harmonic generation (SHG) image of collagen fibers in a mouse aorta; The image size was 30 × 30 μm^2. (b) A power spectrum image (PSI) obtained using 2 dimensional fast Fourier transform (2D-FFT) analysis of the image (a); (c) Probability distribution of fiber orientation from image (b) and its Gaussian fit; Variables P_{base}, P_{peak}, $\alpha_{average}$, and σ are fitting constants from Eq. (5).

Fig. 4 Typical multiphoton microscopy (MPM) images of a rabbit thoracic aorta stretched at physiological stretch ratios

Elastin (a–c), collagen (d–f), and their merged images (g–i) in the circumferential–longitudinal plane are shown at various radial positions. Elastin and collagen are indicated in red and green, respectively (g–j). Z indicates the relative position from the luminal surface of internal elastic lamina (IEL) in μm; IEL (a, d, and g), the first smooth muscle rich layers (SML; b, e, and h), and the second elastic lamina (EL; c, f, and i) from the intimal side; Insets in panels a, d, and g show enlarged views of white rectangular areas. A typical image in the longitudinal–radial plane (j) obtained by reslicing the images in the circumferential–longitudinal plane (a-i). A typical merged image of cell nuclei (green to yellow, arrows) and elastin (red) in the longitudinal–radial plane (k); This image section was generated using similar procedures to

those for (j). The length scale in (i) applies to (a)–(i). See supplemental movie S1 for details of (a)–(i).

Fig. 5 Three-dimensional (3D) microstructure of elastin and collagen fibers in a rabbit thoracic aorta stretched at physiological stretch ratios

(a–c) Typical images of collagen (a, green) and elastin (b, red) fibers and merged images (c) in the circumferential–longitudinal plane; Images were taken at 9 μm from the IEL. (d) A resliced and projected image in a longitudinal–radial plane of the image shown in (a–c); Scale bar = 1.24 μm. (e) Deviation of center point displacement of fibers in longitudinal and radial directions. (f) Waviness of fibers; Data in (g) and (f) were obtained from 27 segments of fibers in the thoracic aortas obtained from three rabbits. See supplemental movie S2 for detailed structures of fibers.

Fig. 6 Typical images of collagen fibers at low (left) and high (right) pressure in the mid-region in the media of a mouse thoracic aorta

Typical SHG light images at 20 and 120 mmHg (top row), enlarged images of 30 × 30 μm^2 areas from dark and bright regions (middle row), and their PSI images from 2D-FFT analysis (bottom row) are shown. Dark and bright regions correspond with SMLs and ELs, respectively.

Fig. 7 Changes in collagen fiber orientation in media from mouse thoracic aorta during pressurization

Images were generated from the 2D-FFT images shown in Fig. 6. Probability distributions of fiber orientation (a), average angle $\alpha_{average}$ (b), base level P_{base} (c), peak value P_{peak} (d), and standard deviations (SD) σ (e) are summarized. The parameters P_{base} and P_{peak} correlated significantly with pressure in bright and dark regions, whereas the parameters $\alpha_{average}$ and σ did not. Dark and bright regions correspond with SMLs and ELs, respectively; *N*, numbers of mice; *n*, numbers of local areas.

Fig. 8 Schematic of possible explanations for differences in waviness of collagen fibers between the ELs and SMLs during pressurization

Differences in waviness can be caused by differences in stiffness around collagen fibers in ELs and SMLs (a) or by differences in shear deformation in the circumferential direction between the ELs and SMLs (b). The inset image in (b) shows a typical collagen fiber in the circumferential–radial plane; the collagen fiber in the SML bridges two collagen fibers in ELs (arrow).

Fig. 9 Comparison of SHG (collagen) and autofluorescence (elastin) images from rabbit and mouse thoracic aortas at 80 mmHg; Bar = 50 μm.

Figure 1

Click here to download Figure Fig1_ExperimentalSetup_v2.tif

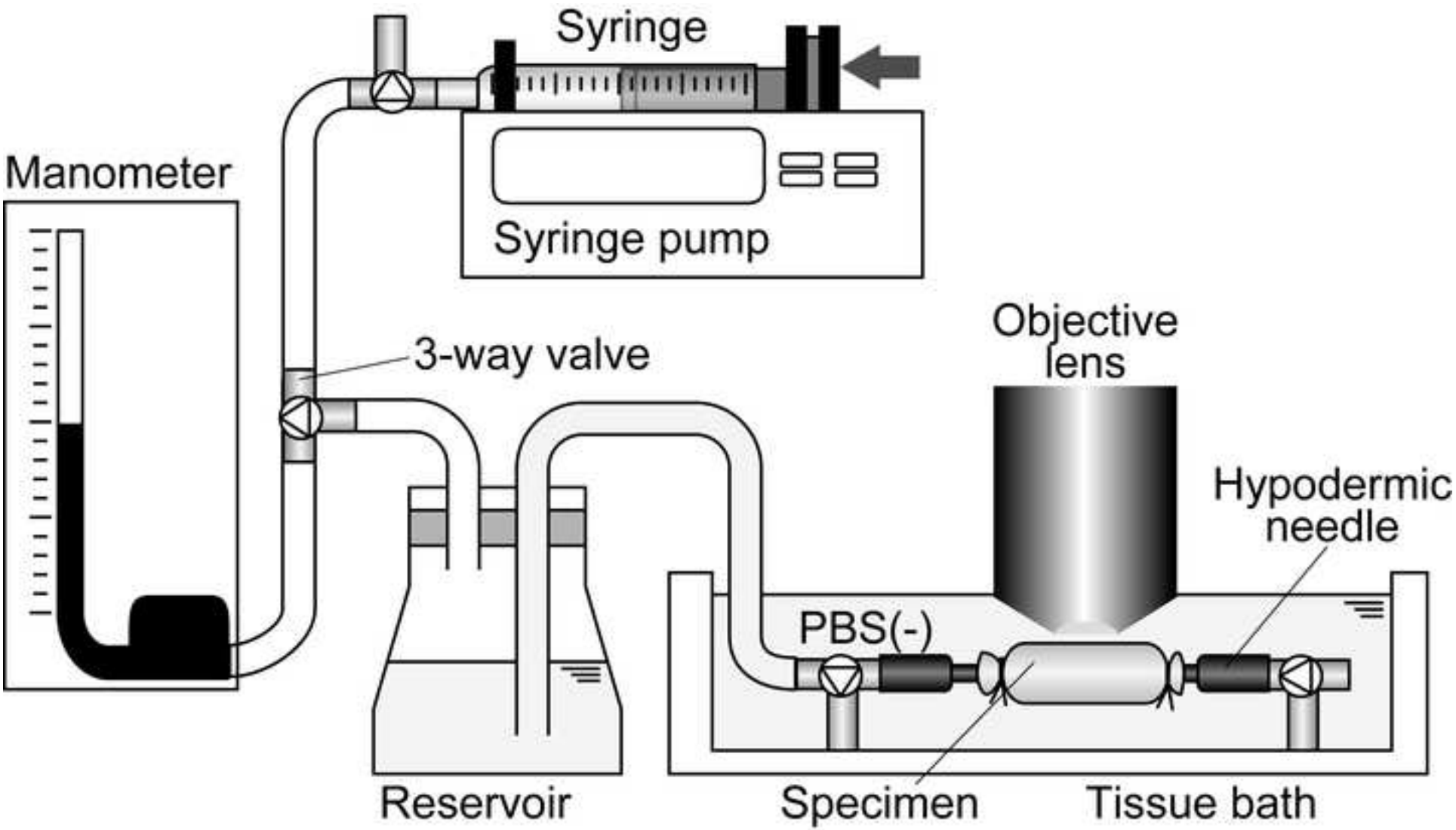

Figure 2

Click here to download Figure Fig2_ResliceExplanation_v3.tif

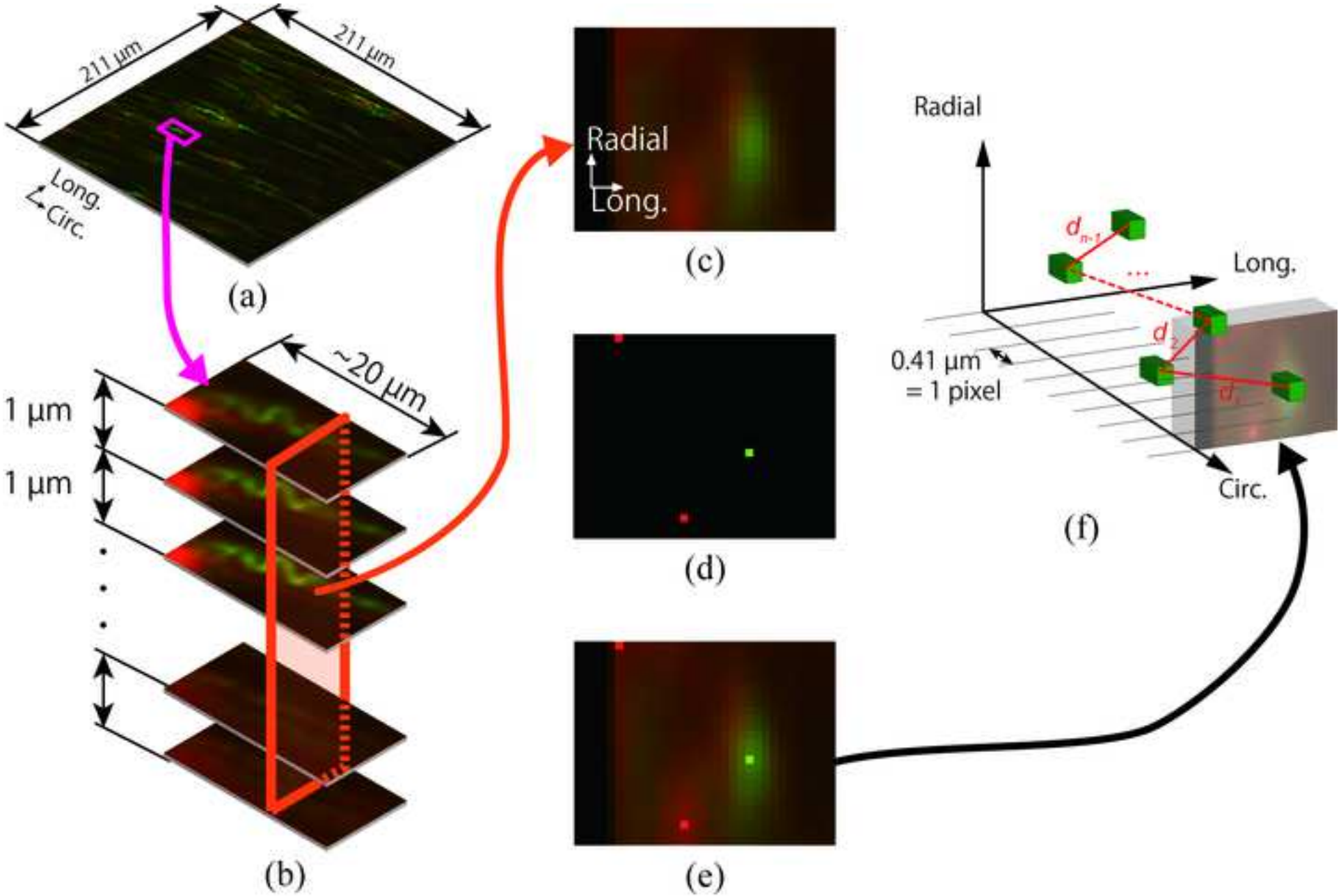

Figure 3

Click here to download Figure
Fig3_FiberDistributionExplanation_v2.tif

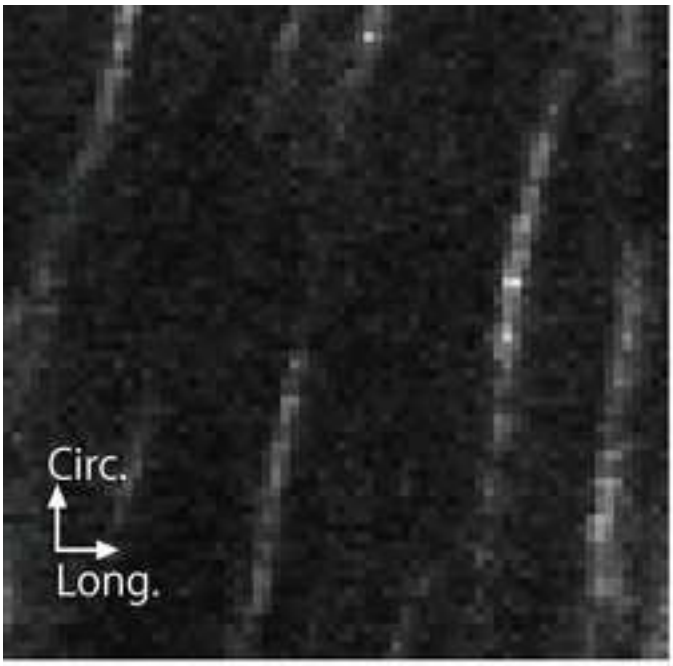

(a)

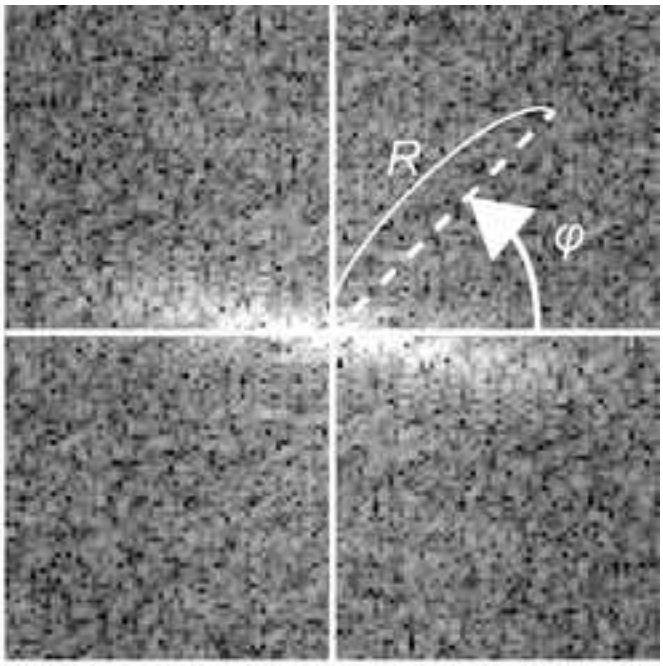

(b)

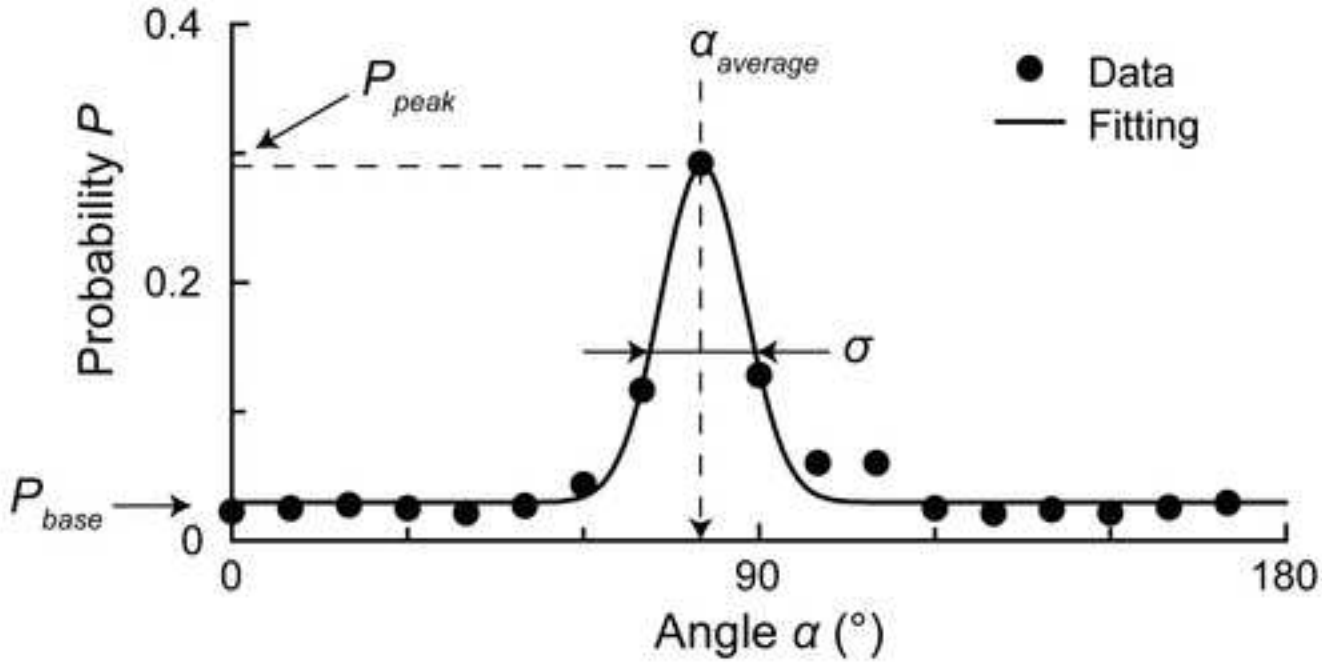

(c)

Figure 4

Click here to download Figure Fig4_Col-ElaImages_v4.tif

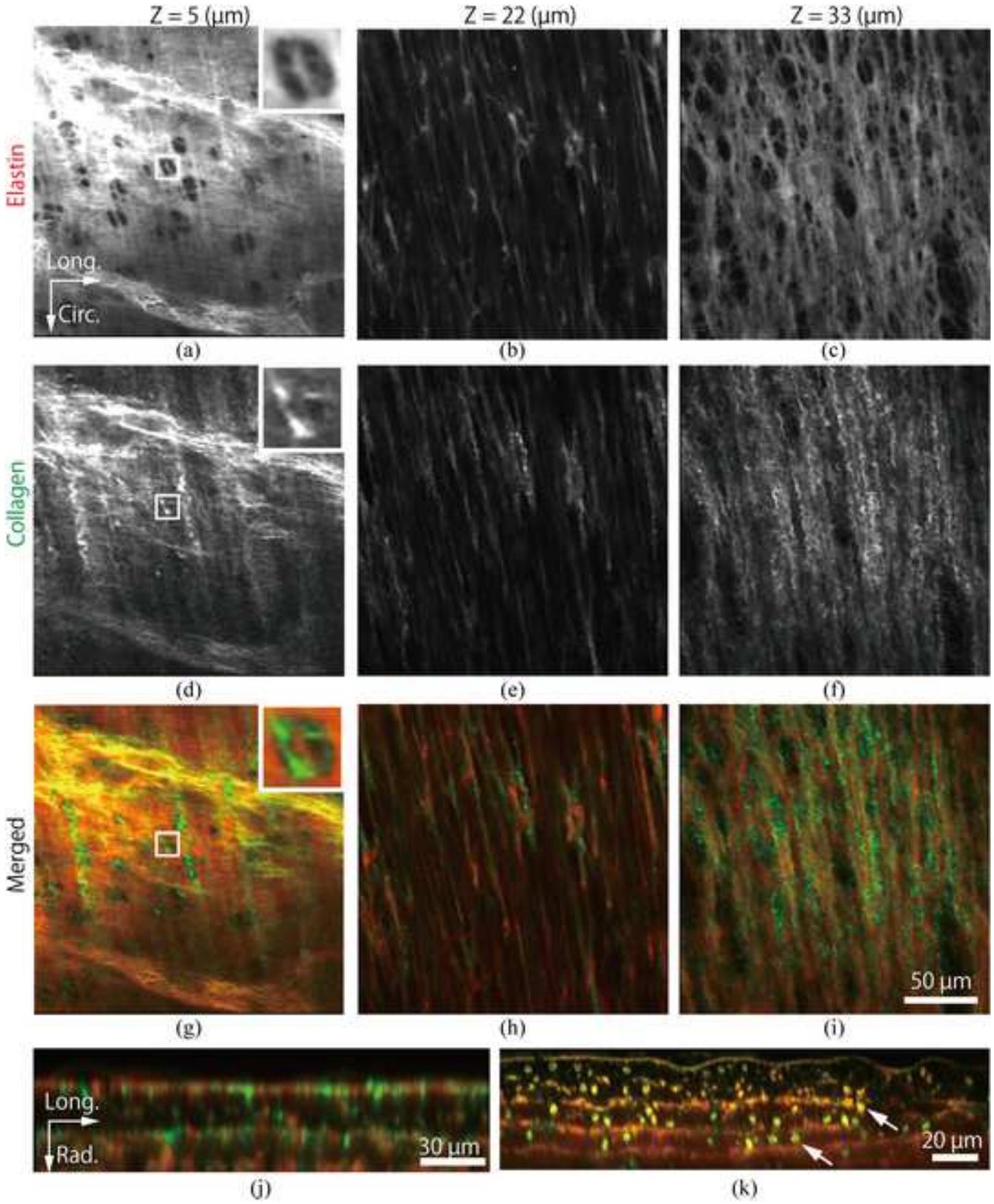

Figure 5

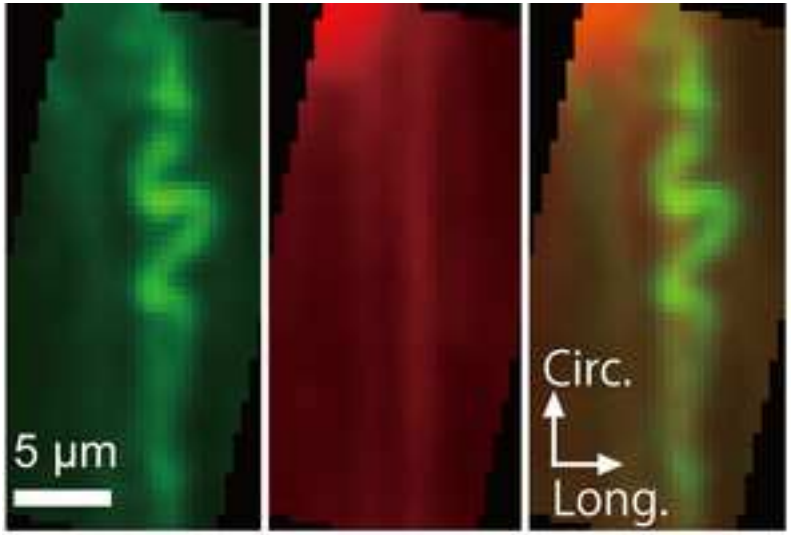

(a) (b) (c)

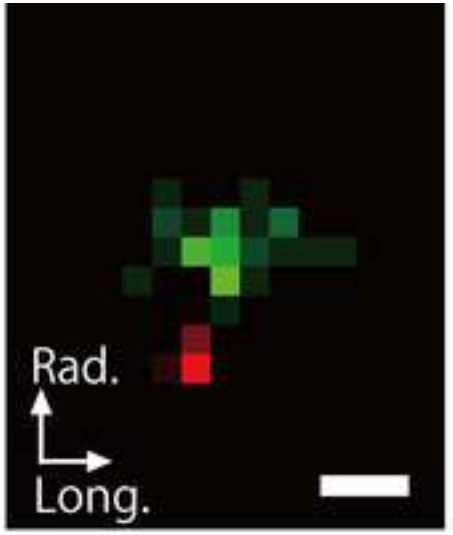

(d)

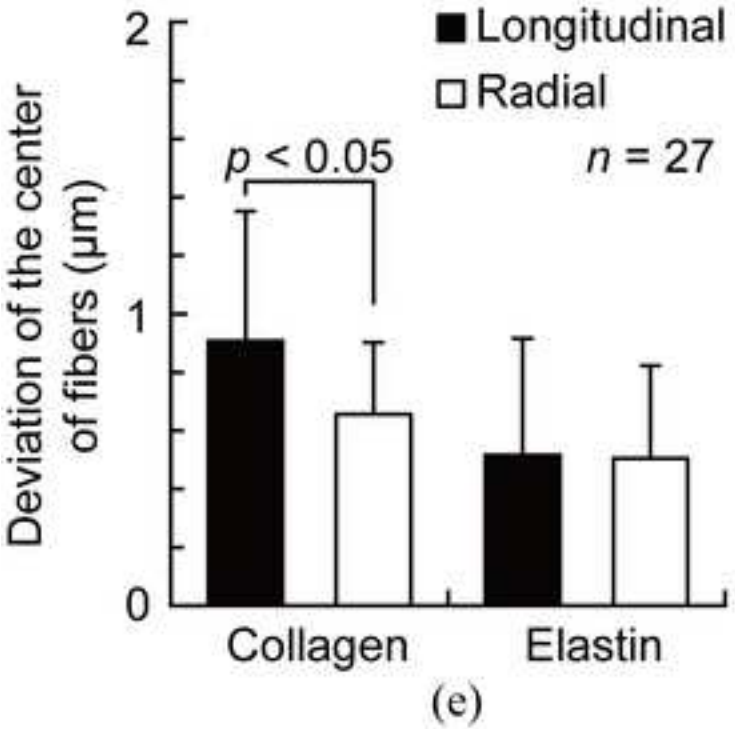

(e)

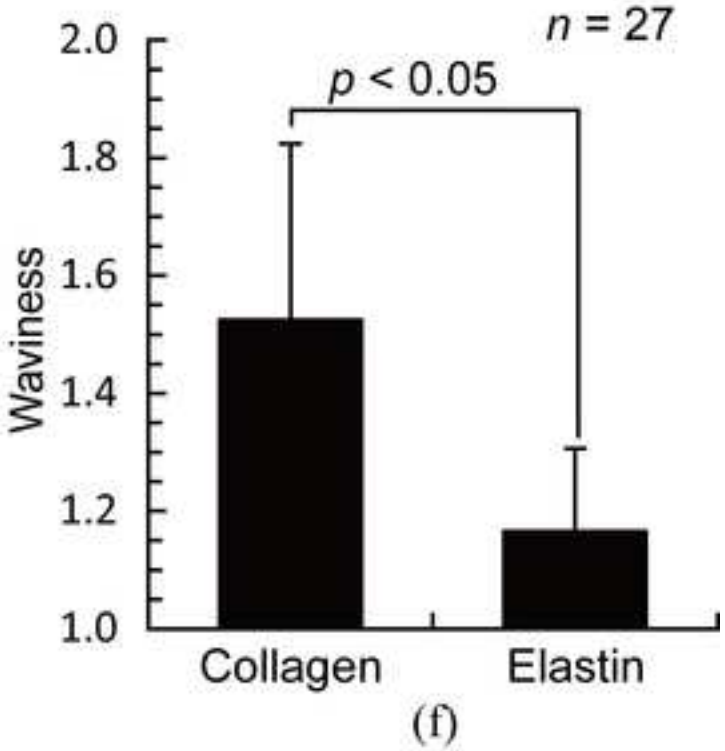

(f)

Figure 6

Click here to download Figure Fig6_HighLowIntensity_v2.tif

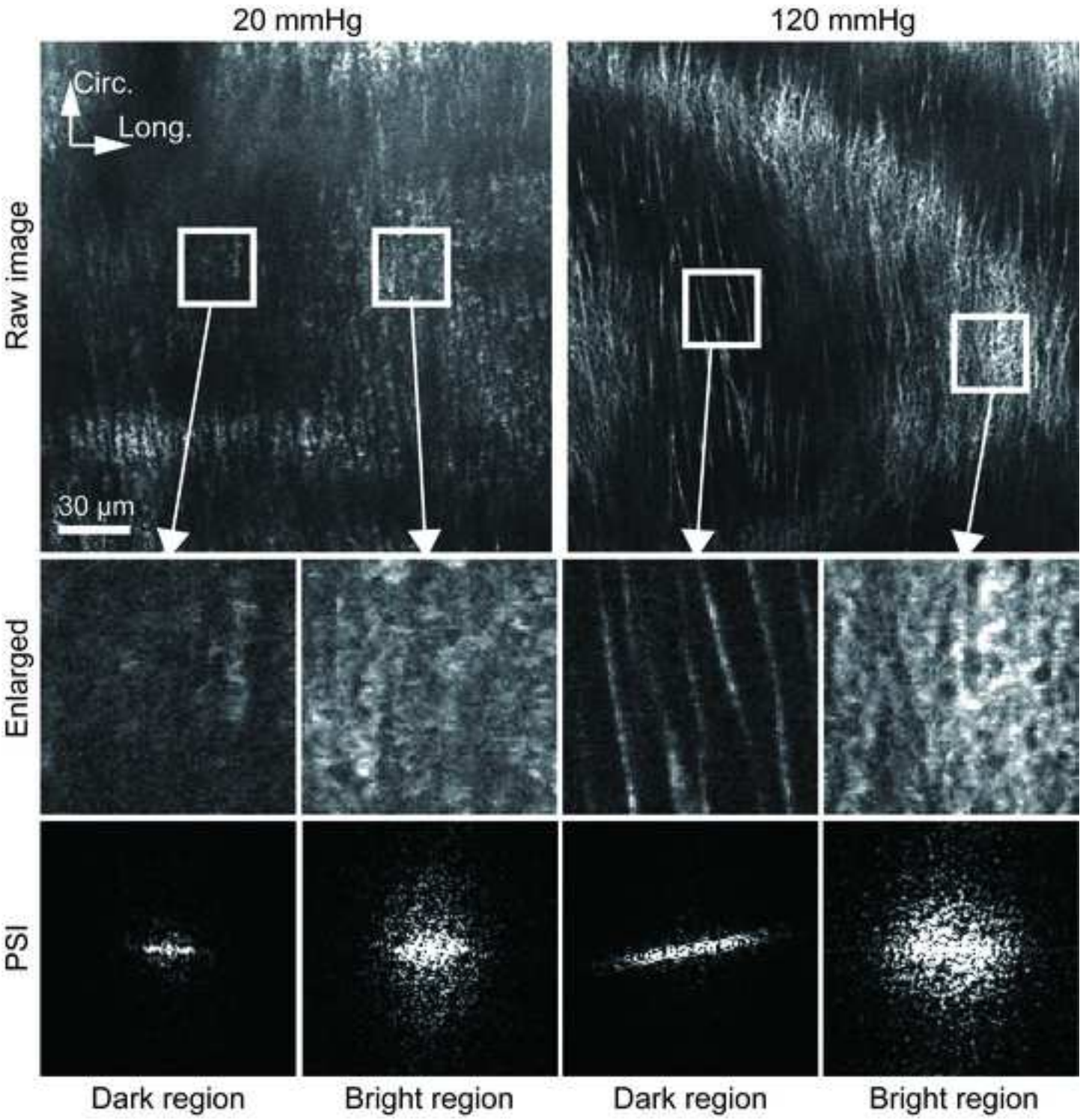

Figure 7

Click here to download Figure
Fig7_HighLowIntensity_Analysis_v4.tif

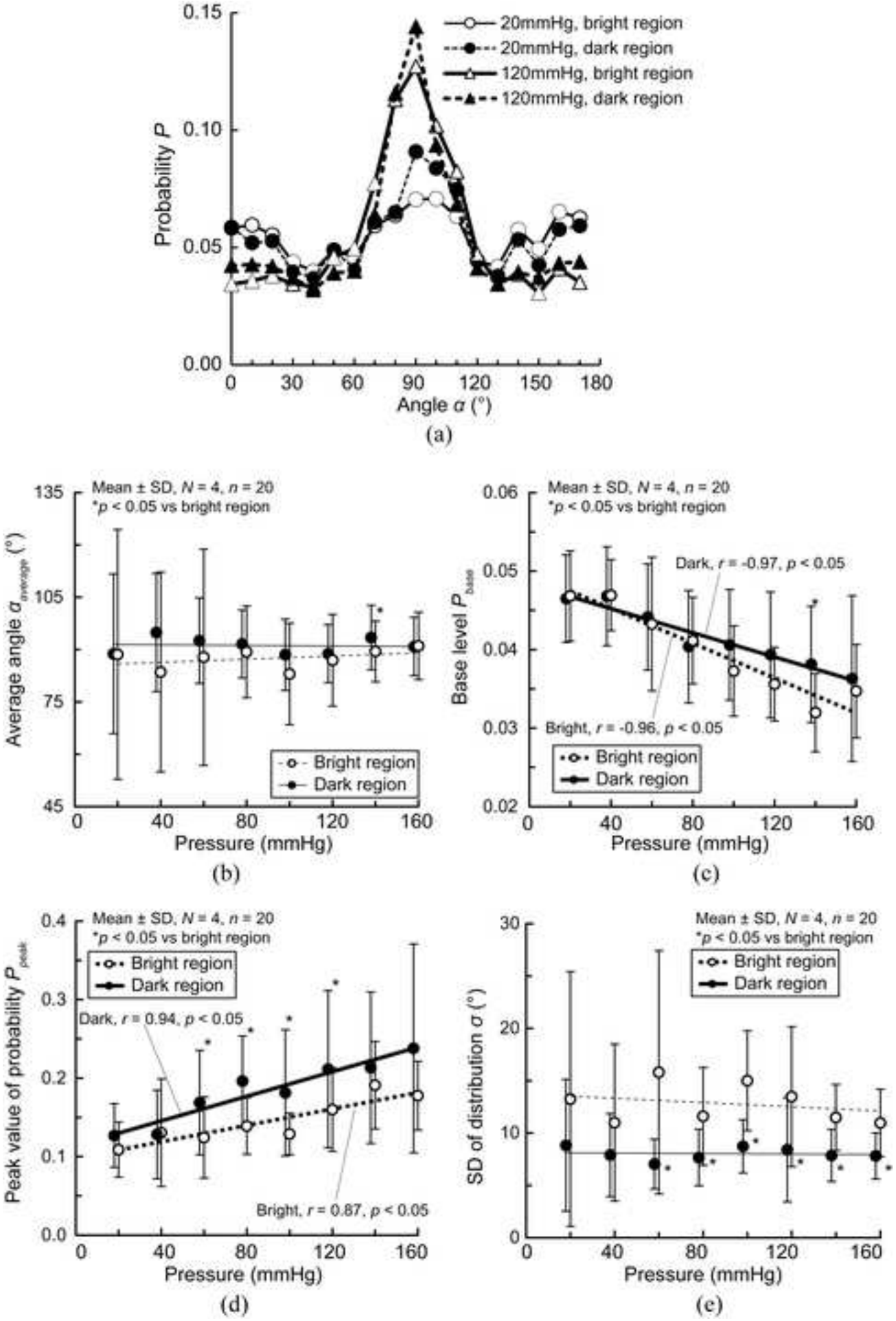

Figure 8

Click here to download Figure Fig8_Model of difference in waviness_v2.tif

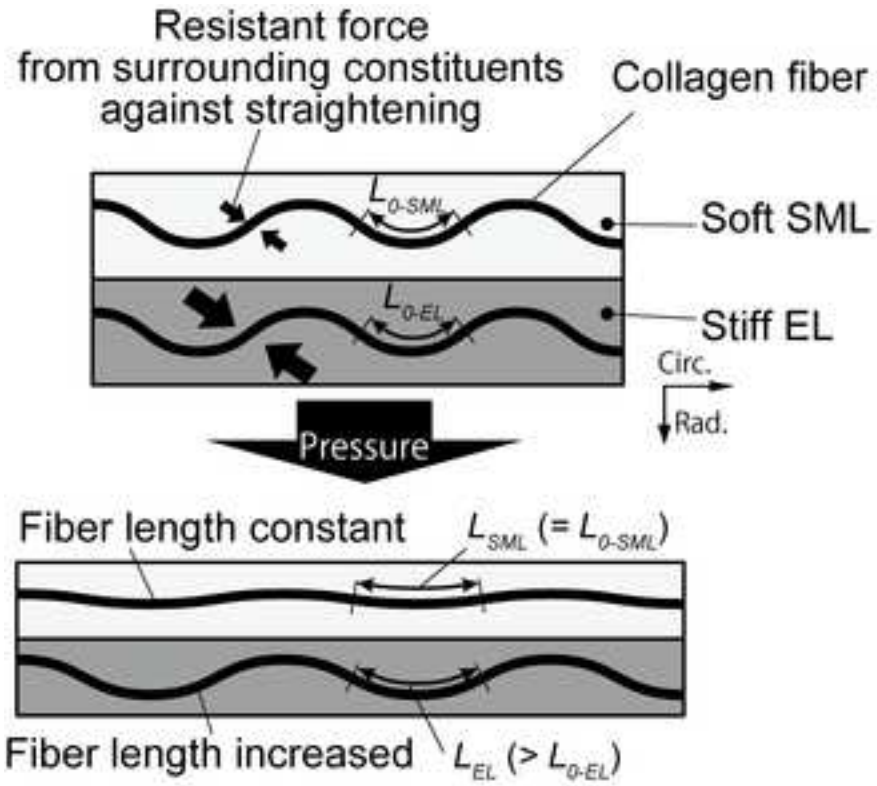

(a)

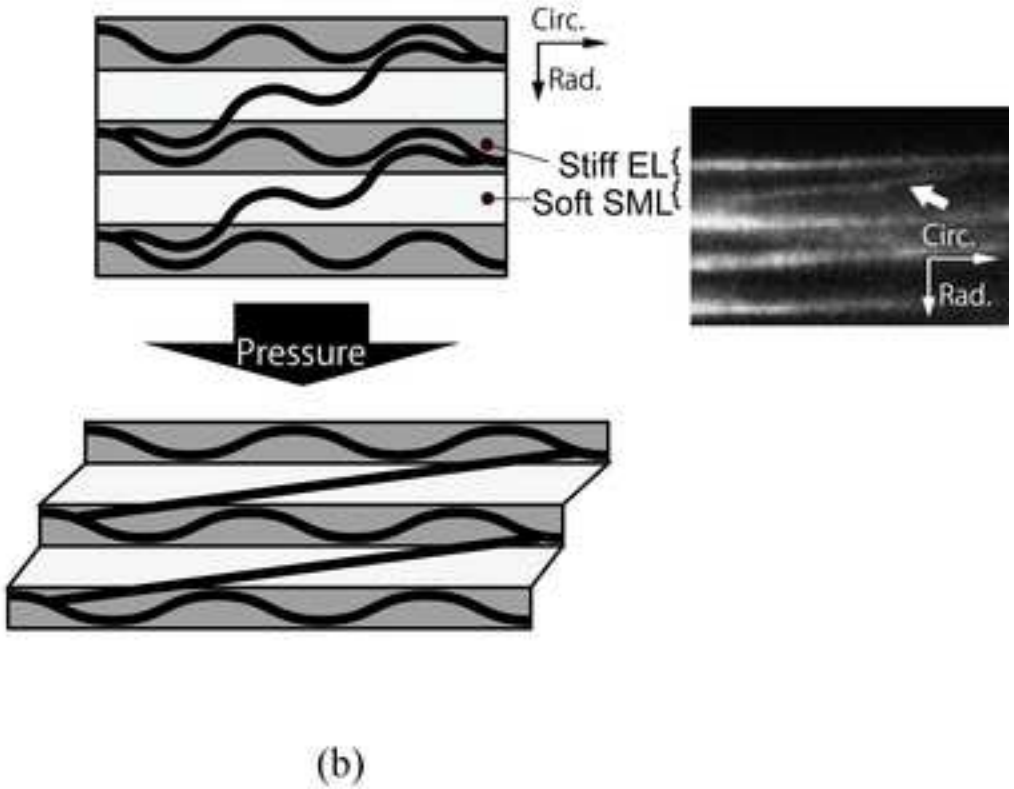

(b)

Figure 9

Click here to download Figure
Fig9_DifferenceInMouseAndRabbit_v2.tif

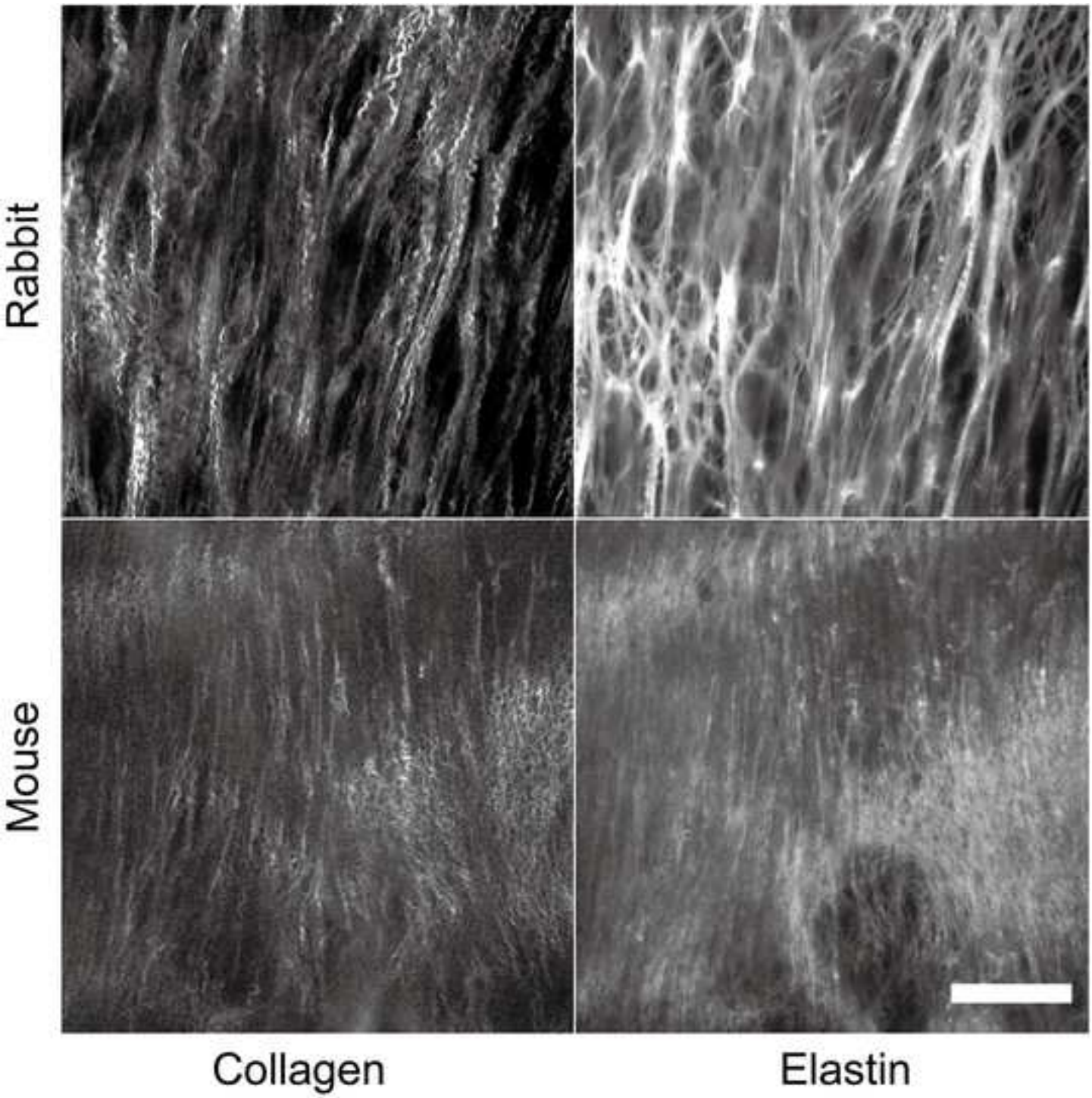

Supplemental Materials

S1. Confirmation of optical setting to observe elastin and collagen fibers

We first confirmed that we can visualize elastin and collagen fibers simultaneously and independently using our experimental setup. Bovine nuchal ligaments obtained at a local butcher were purified for elastin by autoclaving at 118°C for 8 h (Lillie et al. 1994). Tail tendon of Wister rat was used as collagen fiber sample. Rabbit thoracic aortas were prepared as stated in "Sample preparation" subsection in the Materials and Methods section. These specimens were observed as stated in "Multiphoton and SHG microscopy" subsection in the Materials and Methods section except that specimens were observed through low-magnification objectives (UMPLFL, NA = 0.3, Olympus).

Figure S1 shows typical images of autofluorescence and SHG light of bovine nuchal ligament, rat tail tendon, and rabbit thoracic aorta. Images of the elastin and the collagen fibers were basically acquired under the same condition such as exposure time, sensitivity of detector adjustment, and gain, except that SHG image of rat tail tendon was acquired with lower sensitivity because its intensity was too high. The autofluorescence image of the rat tail tendon and the SHG image of the bovine nuchal ligament showed negligibly low intensity in our experimental setup, indicating that elastin and collagen fibers can be clearly distinguished in this setup. Fibers were found in both autofluorescence and SHG images of aortic media and they did not colocalize at all, indicating that elastin and collagen fibers in the aortic media were independently detected.

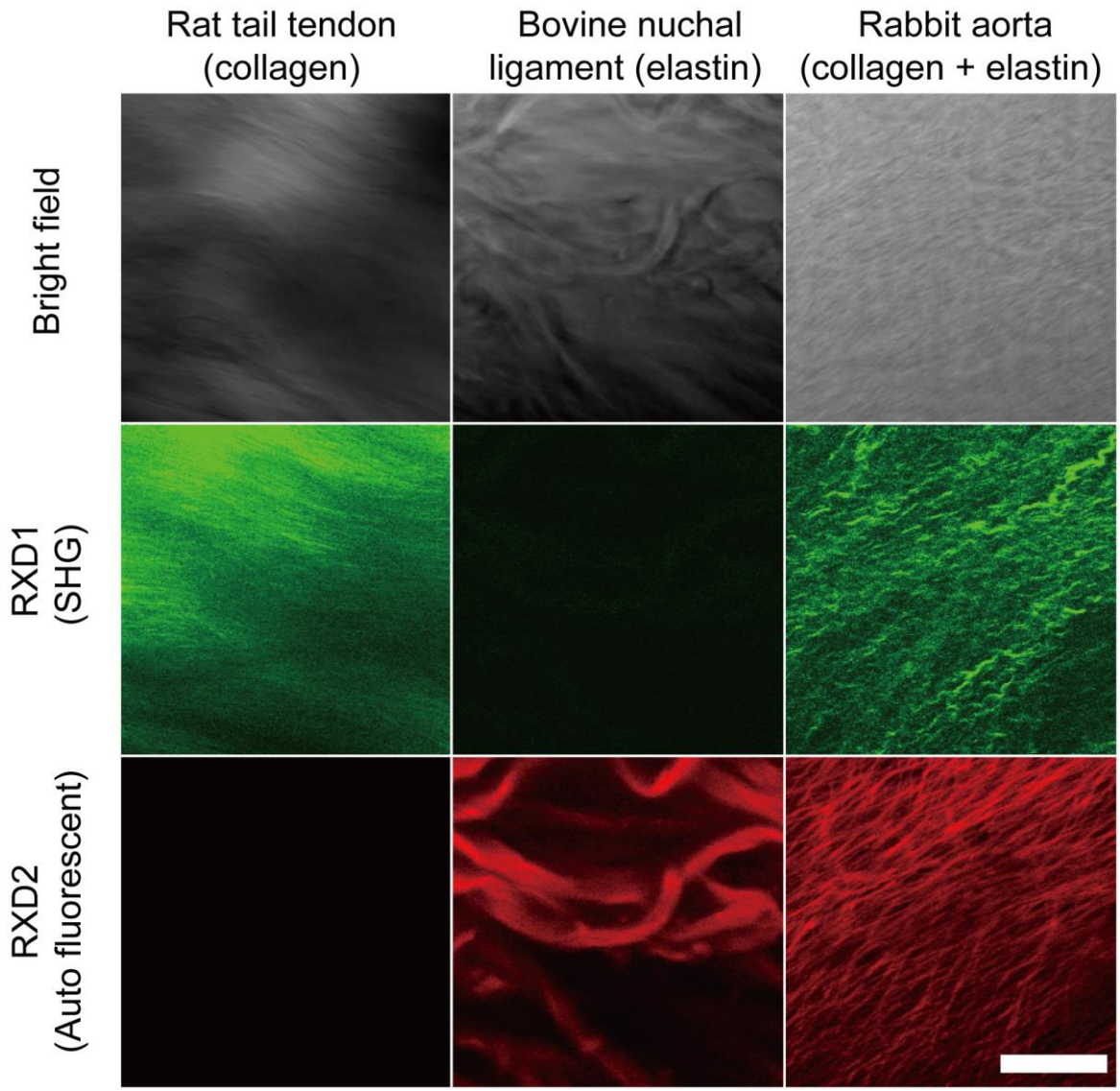

Fig. S1 Typical images of elastin and collagen fibers obtained in the present experimental setup. Bar = 200 μm.

S2. Evaluation of waviness using 2D FFT

To evaluate the changes in waviness of fibers, we generated test images having two identical fibers in each image as shown in Fig. S2(a). Fibers were modeled as sine waves with the same frequency with different amplitude. Waviness W was calculated as length of a sine wave, which was calculated by summing all infinitesimal distance between two points on the curve, divided by distance between the two ends using Microsoft Excel. By applying 2D FFT to these images, the probability distribution of fiber orientation was obtained as shown in Fig. S2(b). The distribution gradually becomes flat and the parameter P_{peak} and σ in Eq. (5) decrease and increase, respectively, with increase in the waviness W from 1.00 to 1.56. We thus used parameters P_{peak} and σ mainly as indices of waviness.

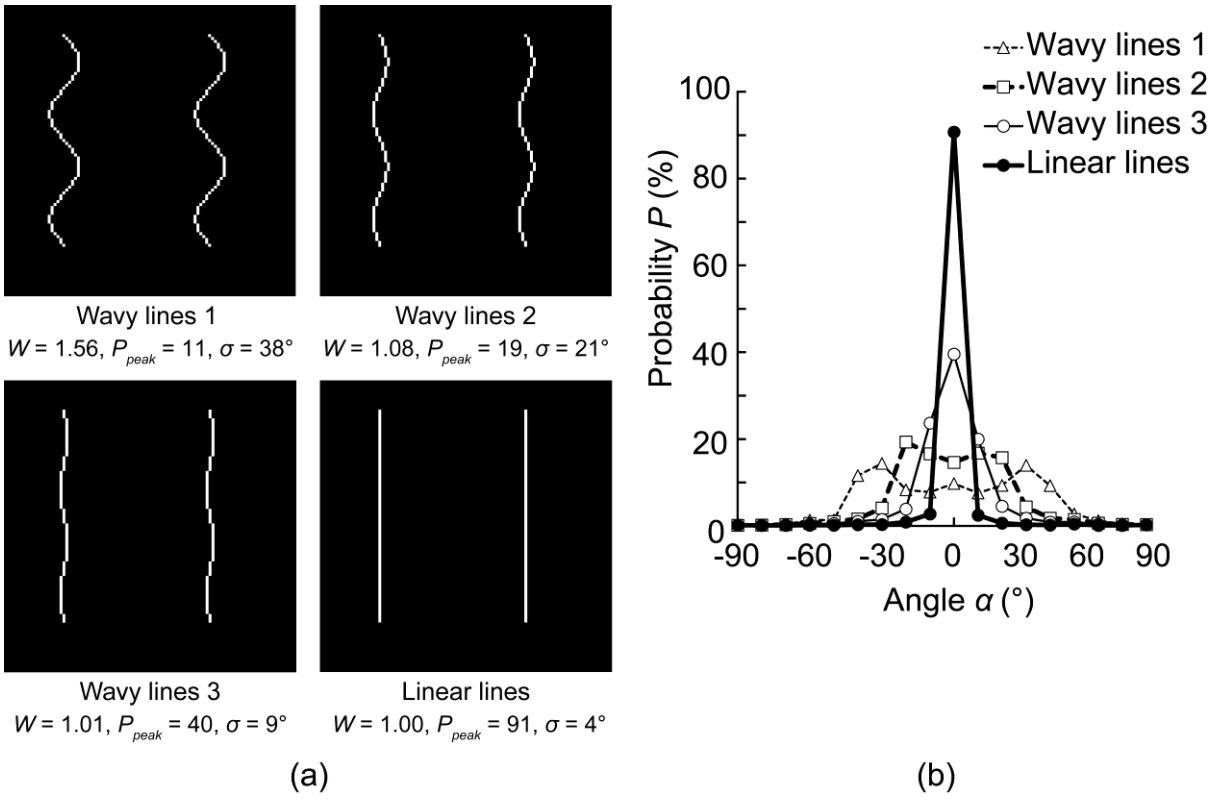

Fig. S2. Test images with two fibers (a) and their probability distributions as to fiber direction (b). The horizontal direction in (a) corresponds to 0° in (b). For parameters P_{peak} and σ in (a), see Fig. 3 and Eq. (5).

S3. An image of cell nuclei along with elastin and collagen fibers in the longitudinal-circumferential plane

To determine EL and SML, cell nuclei in rabbit thoracic aorta were stained with Hoechst 33342. As shown in longitudinal-radial plane (Fig. 4k), cell nuclei were confirmed to be observed in low intensity region of elastin and collagen fibers even in longitudinal-circumferential plane (Fig. S3). Therefore, low and high intensity regions were thought to be SML and EL, respectively.

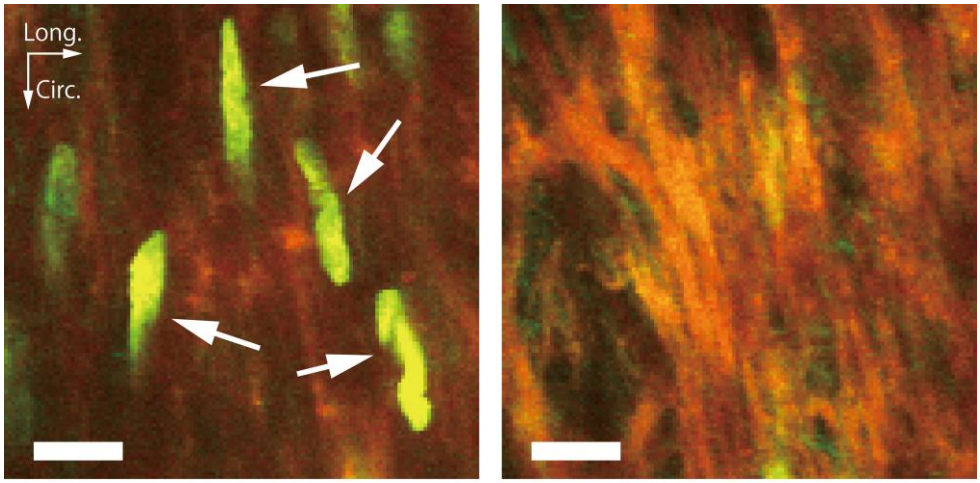

(a) (b)

Fig. S3. Typical images of collagen (green) and elastin (red) along with cell nuclei (yellow to green, some of them are indicated with arrows) stained with Hoechst 33342. Cell nuclei were found in (a) but not in (b), indicating that areas in (a) and (b) correspond to SML and EL, respectively. Bars = 10 μm.

S4. Difference in fiber undulation of collagen fibers between EL and SML in rabbit thoracic aorta using 2D-FFT.

As analyzed in Fig. 7 for mouse aortas, fiber orientation in the rabbit thoracic aorta was evaluated using the parameters P_{base}, P_{peak}, $\alpha_{average}$, and σ in Eq. (5) to compare the fiber orientation in SML and EL. It should be noted that their images were obtained from only its intimal side. Nine 30 × 30 μm^2 areas in ELs and SMLs were selected perpendicular to the radial direction in each set of 3D images like Fig. 4 obtained from rabbit thoracic aortas, and FFT analysis was performed as stated in the MATERIALS AND METHODS section.

Figure S4 shows probability distributions of collagen fiber orientations obtained from rabbit aortas. Parameters P_{peak} (28.6% ± 0.1%) and P_{base} (2.9% ± 0.0%) in dark regions (SMLs) were significantly higher and lower, respectively, than in bright regions (ELs) (P_{peak} = 19.3% ± 0.1%, P_{base} = 3.8% ± 0.0%), although the difference was insignificant in σ (8.4° ± 4.6° for SMLs *vs* 9.5° ± 5.2° for ELs) and $\alpha_{average}$ (99.0° ± 4.9° for SMLs *vs* 100.4° ± 5.2° for ELs). These indicate that collagen fibers become less wavy in SMLs than in ELs at physiological state. These results support that collagen fibers in SMLs less undulated more than those in ELs as obtained in mouse aorta.

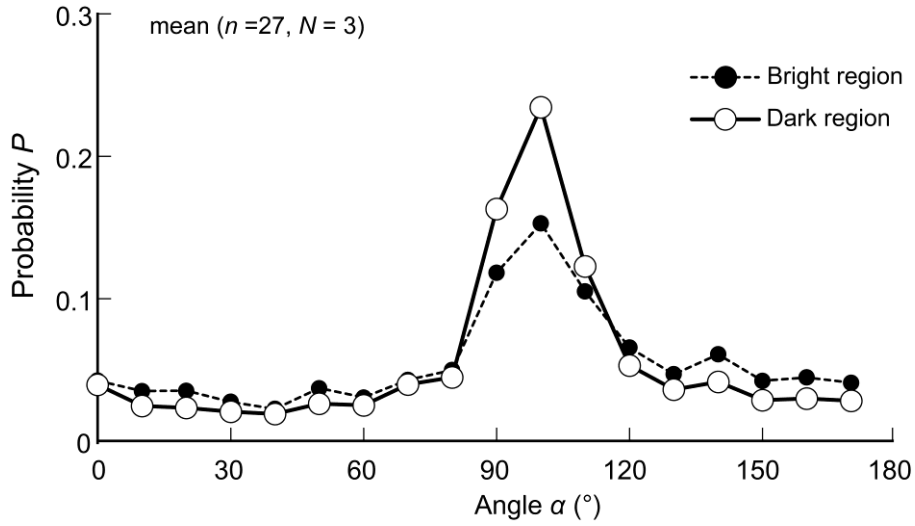

Fig. S4. Probability distributions of orientation of collagen fibers obtained from rabbit thoracic aorta. *N*, number of animals; *n*, number of image area analyzed.

S5. Changes in orientation of elastin fibers in media from mouse thoracic aorta during pressurization.

Probability distributions of elastin fiber orientation were obtained as shown in Fig. 7 for collagen fibers. Differences in distributions of elastin fiber orientation were evaluated from autofluorescent images (Fig. S5a and S5b) using the parameters P_{base}, P_{peak}, $\alpha_{average}$, and σ in Eq. (5). Distributions of fiber orientations (Fig. S5c) showed that most elastin fibers were aligned to 90°, which was confirmed by relative insensitivities of angles at maximum alignment $\alpha_{average}$ to pressure and region (Fig. S5d). This indicates that the orientation of elastin fibers is predominantly circumferential, which is similar to collagen. The base level of the fitted Gaussian function P_{base} and its peak P_{peak} decreased and increased, respectively, with pressure increases in both regions though their correlation coefficients were significant only in the dark region (SML; Fig. S5e, S5f). In collagen, P_{base} and P_{peak} correlated significantly with increase in the pressure in both regions (Fig. 7). Furthermore, unlike collagen, significant difference between EL and SML for σ was only found at 40 and 80 mmHg (Fig. S5g). Compared to collagen, elastin fibers are less wavy as shown in Fig. 5f. Fibers with smaller waviness have larger P_{peak} value (Fig. S2). Relative insensitiveness of P_{peak} value of elastin to an increase in pressure (Fig S5) might be caused because elastin fibers were less wavy and P_{peak} value had already reached a plateau. Either way, change in waviness was larger in SML than EL, which is similar to changes in collagen.

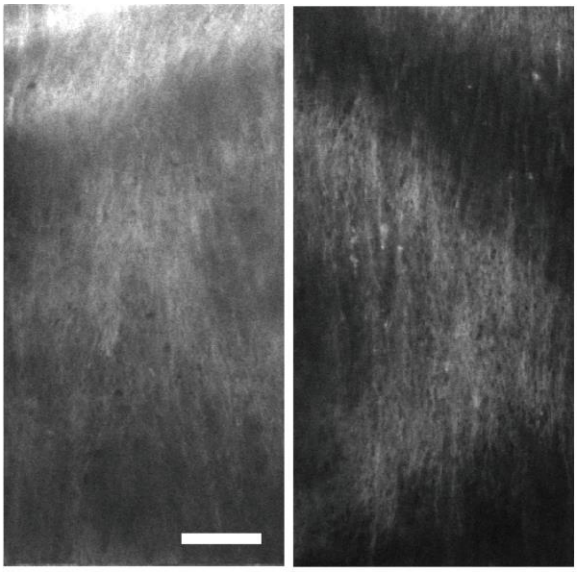

(a) (b)

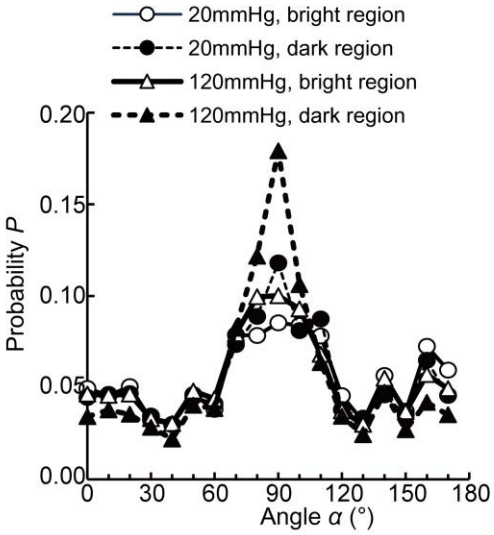
20mmHg, bright region
20mmHg, dark region
120mmHg, bright region
120mmHg, dark region
Probability P
Angle α (°)

(c)

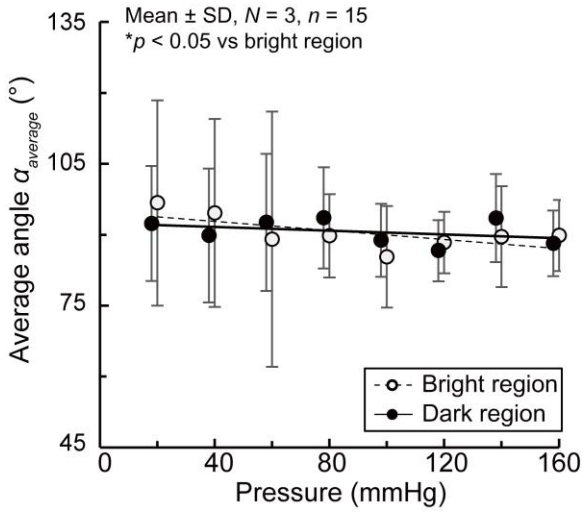
Mean ± SD, N = 3, n = 15
*p < 0.05 vs bright region
Average angle α_average (°)
Bright region
Dark region
Pressure (mmHg)

(d)

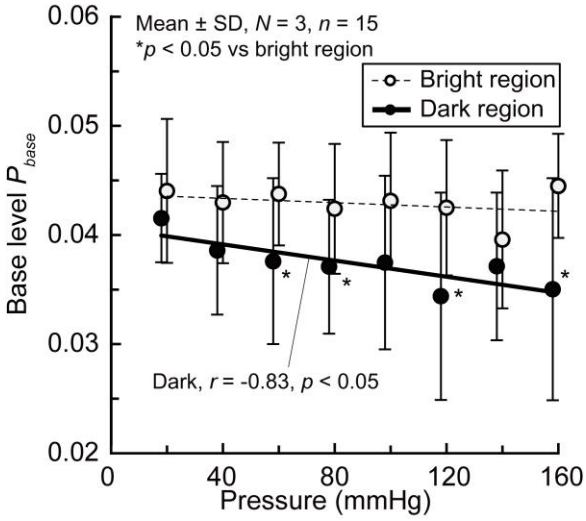
Mean ± SD, N = 3, n = 15
*p < 0.05 vs bright region
Base level P_base
Bright region
Dark region
Dark, r = -0.83, p < 0.05
Pressure (mmHg)

(e)

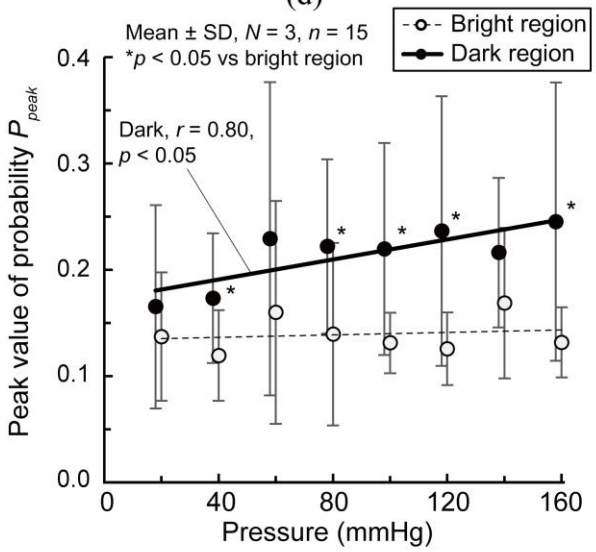
Mean ± SD, N = 3, n = 15
*p < 0.05 vs bright region
Bright region
Dark region
Dark, r = 0.80,
p < 0.05
Peak value of probability P_peak
Pressure (mmHg)

(f)

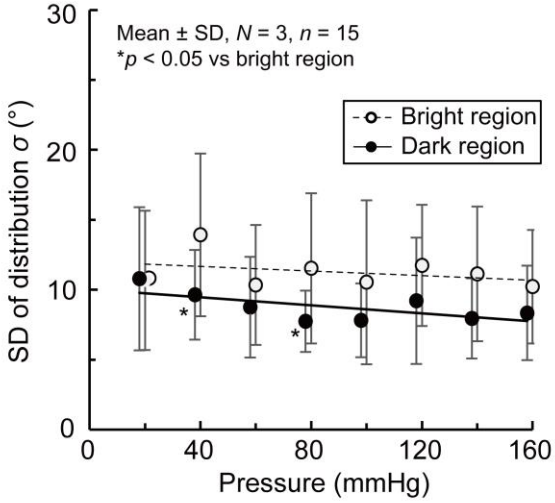
Mean ± SD, N = 3, n = 15
*p < 0.05 vs bright region
Bright region
Dark region
SD of distribution σ (°)
Pressure (mmHg)

(g)

Fig. S5. Changes in orientation of elastin fiber in media from mouse thoracic aorta during pressurization

Typical autofluorescent images of elastin at (a) 20 mmHg and (b) 120 mmHg; Bar in (a) corresponds to 30 μm. Probability distributions of orientation of elastin fiber (c), average angle $\alpha_{average}$ (d), base level P_{base} (e), peak value P_{peak} (f), and standard deviations (SD) σ (g) are summarized. The parameters P_{base} and P_{peak} correlated significantly with pressure in dark region, whereas the parameters $\alpha_{average}$ and σ did not. Dark and bright regions correspond to SMLs and ELs, respectively; *N*, numbers of mice; *n*, numbers of local areas.

S6. Shear deformation in the aortic wall during pressurization.

In a previous study (Sugita et al. 2003), we studied the difference in deformation between the ventral and dorsal sides of the rabbit thoracic aorta during pressurization. For this purpose, four small needles were stuck perpendicularly into the aortic wall at equal intervals on a circumference and image of the needles were captured from the longitudinal direction. During this process, we noticed that artery wall shows marked shear deformation during pressurization. Figure S6 shows typical images of needles captured at 40, 80, and 120 mmHg, along with their SD image obtained by calculating SD at each pixel from source images. The SD image clearly shows rotation of needles, i.e., shear deformation of the wall during pressurization. The angle changed significantly as the specimens pressurized from 40 mmHg to 120 mmHg ($P<0.05$, paired t-test) and absolute value of the change was 9° ± 8° (mean ± SD, $n = 48$ from 12 samples). Twenty-seven out of 48 needles rotated more than 5°. Thus, shear deformation may be very common in the aortic walls.

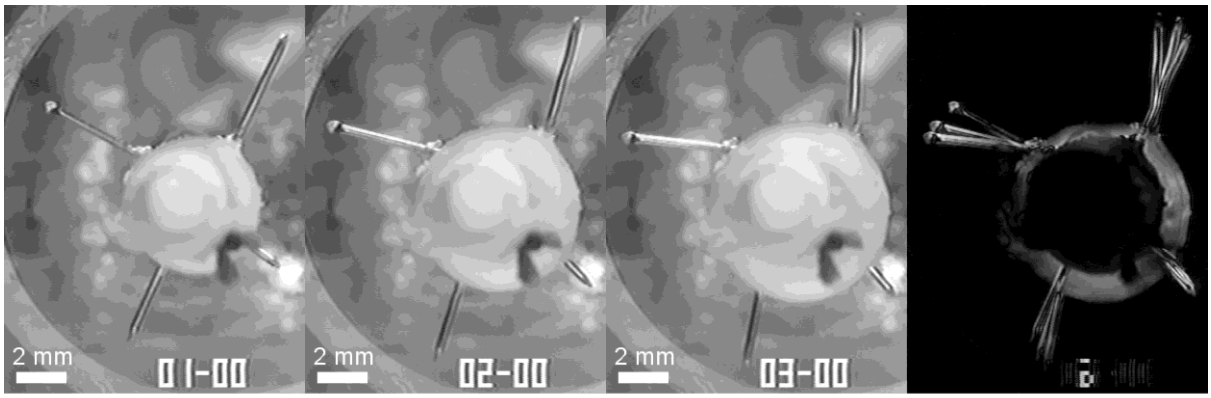

(a) 40 mmHg (b) 80 mmHg (c) 120 mmHg (d) SD

Fig. S6. Changes in angle of needles during pressurization. Images of needles were captured from the longitudinal direction.

Movie 1

Merged image of elastin (green) and collagen fibers (red) in stack slices. Upper left indicator shows position in radial direction from the luminal surface of IEL in μm.

Movie 2

A 3D reconstructed image of typical elastin (red) and collagen (green) fibers. The collagen fiber is undulated, while elastin fibers are almost straight.

References

Lillie MA, Chalmers GW, Gosline JM (1994) The effects of heating on the mechanical properties of arterial elastin Connect Tissue Res 31:23-35

Sugita S, Matsumoto T, Sato M (2003) Local strain measurement of arterial wall based on longitudinal observation Transactions of the Japan Society of Mechanical Engineers Series A 69:43-48

Movie S1

Click here to access/download

Supplemental Video/Audio File

Movie S1.avi

Movie S2

Click here to access/download

Supplemental Video/Audio File

Movie S2.avi